Exploring the Reduction Mechanism of ^{99}Tc(VII) in $NaClO_4$: A Spectro-Electrochimical Approach

Rodriguez Hernandez, D. M.; Mayordomo, N.; Parra-Puerto, A.; Schild, D.; Brendler, V.; Stumpf, T.; Müller, K.;

Originally published:

June 2022

Inorganic Chemistry 61(2022)26, 10159-10166

DOI: https://doi.org/10.1021/acs.inorgchem.2c01278

Exploring the reduction mechanism of ^{99}Tc(VII) in $NaClO_4$: A spectro-electrochemical approach

Diana M. Rodríguez [1], Natalia Mayordomo [1], Andrés Parra-Puerto [2], Dieter Schild [3], Vinzenz Brendler [1], Thorsten Stumpf [1], Katharina Müller [1*]*

[1] Institute of Resource Ecology, Helmholtz-Zentrum Dresden – Rossendorf e.V., Bautzner Landstraße 400, 01328 Dresden, Germany.

[2] Department of Chemistry, Imperial College London, London, SW7 2AZ, United Kingdom.

[3] Institute for Nuclear Waste Disposal, Karlsruhe Institute of Technology (KIT), Hermann-von-Helmholtz-Platz 1, 76344 Eggenstein-Leopoldshafen, Germany.

* Corresponding authors: n.mayordomo-herranz@hzdr.de (N. Mayordomo, Phone: +49 351 260 2076), k.mueller@hzdr.de (K. Müller, Phone: +49 351 260 2439)

ABSTRACT

Technetium (Tc) is an environmentally relevant radioactive contaminant whose migration is limited when Tc(VII) is reduced to Tc(IV). However, its reaction mechanisms are not well understood yet. We have combined electrochemistry, spectroscopy, and microscopy (cyclic voltammetry, rotating disk electrode, X-ray photoelectron spectroscopy, Raman and scanning electron microscopy) to study Tc(VII) reduction in non-complexing media: 0.5 mM $KTcO_4$ in 2 M $NaClO_4$ in the pH from 2.0 to 10.0. At pH 2.0, Tc(VII) first gains 2.3 ± 0.3 electrons, following Tc(V) rapidly receives 1.3 ± 0.3 electrons yielding Tc(IV). At pH 4.0-10.0, Tc(IV) is directly obtained by transfer of 3.2 ± 0.3 electrons. The reduction of Tc(VII) produced always a black solid identified as Tc(IV) by Raman and XPS. Our results narrow a significant gap in the fundamental knowledge of Tc aqueous chemistry and are important to understand Tc speciation. They provide basic steps on the way from non-complexing to complex media.

SYNOPSIS

The reduction of Tc(VII) to Tc(IV) in non-complexing media depends on pH. At pH 2, Tc(VII) gains two electrons and consequently Tc(V) gains an additional electron to become Tc(IV); whereas at pH 4-10 Tc(VIII) reduces directly to Tc(IV).

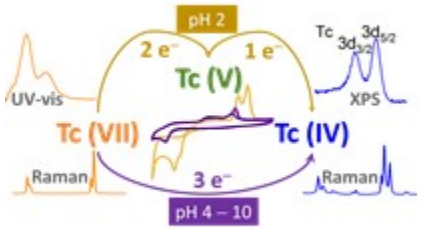

KEYWORDS:

Technetium • Raman spectroscopy • X-ray photoelectron spectroscopy • Non-complexing media • Electrochemistry • Electron transfer

1. INTRODUCTION

Technetium (Tc, Z=43), discovered by Sagré and Perrier in 1937 [1], is the lightest element with no stable isotopes. Among them, the most abundant is ^{99}Tc, a β-particle emitter with a long half-life of 2.14×10^5 years. In the early 60s the application as clinical tracer of the metastable isotope, ^{99m}Tc (half-life of 6.007 h), was first published [2] and, since then, it has been used for the imaging of several organs like the brain and the lungs.

Technetium might occur naturally within the Earth crust originating from spontaneous fission of ^{238}U, neutron-induced fission of ^{235}U, or interactions between molybdenum, ruthenium or niobium and cosmic rays [3]. However, the vast majority of the ^{99}Tc found on Earth is a result of anthropogenic activity such as nuclear energy production and nuclear weapon testing [3,4], as well as the decay product of ^{99m}Tc used in diagnostics [5,6]. In a typical 1 GW nuclear power plant, 21 kg of ^{99}Tc (13.2×10^{15} Bq) are formed annually as fission product [7]; the global Tc production in 2007 was estimated to be 15.1×10^3 kg. Taking this as a rough average, in 2020 there were approximately 4.71×10^5 kg ^{99}Tc, equivalent to 2.963×10^{17} Bq, present on Earth. The majority of Tc waste is still waiting for proper disposal in deep geological repositories that, combining engineered (e.g. vitrified waste, buffer and sealing materials, borehole

fillings) and geological barriers (host-rock) will isolate the radioactive waste from the (hydro)biosphere for up to one million years [7].

To ensure a safe storage, it is of outmost importance to understand Tc chemical behavior to assess its migration in water, which is strongly influenced by its aqueous speciation [8]. Under oxidizing conditions it occurs as pertechnetate, $Tc(VII)O_4^-$, an anion with high water solubility and low to no interaction with geochemical barriers [9,10]. Consequently, an ingress of ground water to the repository under oxidizing conditions – as worst case scenario – will trigger the migration of Tc(VII) to the biosphere. There, it could easily get incorporated into the food chain causing health problems to animals and humans [3,7,11]. Under reducing conditions, Tc(IV) is the most stable oxidation state, which commonly forms a solid, TcO_2, with a low aqueous solubility ($\log K_{sp} = 8.17 \pm 0.05$ [12]). Thus, the reduction of Tc(VII) to Tc(IV) is an effective strategy for technetium immobilization. Recently several Fe(II) minerals have been studied in detail: Iron sulfide in the form of pyrite and marcasite [13–15] chukanovite, [16] magnetite [17,18], or other common systems like layered double hydroxides [19] trigger Tc(VII) reduction and then incorporate, precipitate or adsorb Tc(IV).

Despite the clear relevance of the reduction of Tc(VII) from an environmental and chemical point of view, more than 80 years after the discovery of technetium, its reduction mechanisms in water are not well understood yet [20]. Although several studies have been performed, especially in acidic media [21–23], it is not clear whether it proceeds in a direct three-electron transfer or if there are intermediary oxidation states involved [24–26]. Moreover, there is no systematic study of the effect of pH and ionic strength on the mechanism. There are also some contradictions observed in the literature. For example, Salaria et al.[27,28] propose the reduction from Tc(VII) to Tc(III) passing through Tc(IV), whereas Grassi et al.[29] propose the reduction from Tc(VII) to Tc(IV) with the direct transfer of three electrons, and other authors suggest that the final product would be Tc(IV) with Tc(V) as an intermediary step [30–32]. Moreover, it must be noted that all these previous studies use ions like Cl^- as background electrolytes that are well known to form complexes with technetium [12,33], invalidating such results for a formulation of redox mechanisms in pure water. This seriously hampers the modeling of technetium migration behavior in any compartment of geosphere or ecosphere.

In order to narrow this substantial gap in the understanding of technetium aqueous chemistry, we studied the reduction of Tc(VII) in sodium perchlorate ($NaClO_4$), a stable background electrolyte that does not form complexes with Tc(VII) [12] and, in consequence, minimizes artefacts in reactive transport models for Tc in aqueous media. This will provide valuable reference data for more complex systems in the

future. Experiments were performed at $2.0 \leq pH \leq 10.0$ in order to determine the effect of pH on the mechanism and the reaction products. To get comprehensive molecular understanding on the Tc reduction chemistry, we combined electrochemical (cyclic voltammetry and rotating disk electrode), spectroscopic (Raman and X-ray photoelectron spectroscopy), and microscopic (scanning electron microscopy) methods.

2. MATERIALS AND METHODS

2.1 Sample preparation

Radiation safety. ^{99}Tc is a β-particle emitter and should be handled only in a dedicated radiochemistry laboratory with specific radiation safety measurements in place.

All solutions were prepared using $K^{99}TcO_4$ (Institute of Radiopharmaceutical Cancer Research at Helmholtz-Zentrum Dresden-Rossendorf), $NaClO_4 \times H_2O$ (purity ≥ 98%, PanReac AppliChem ITW Reagents) and Milli-Q water (resistivity of 18.2 MΩ cm, Water Purified®). In general, 7 mL of 0.5 mM $KTcO_4$ solutions were prepared in 2 M $NaClO_4$ at pH 2.0, 4.0, 6.0, 8.0, 10.0. The concentrations of both $NaClO_4$ and $KTcO_4$ were constant throughout the experiments. The pH was adjusted by adding small amounts (less than 10 µL in total) of $HClO_4$ or NaOH, changes in ionic strength and viscosity were negligible. The pH was measured using a pH meter (pH3110, WTW) with a pH electrode (SI Analytics Blue Line) calibrated with standard pH buffers 4.006, 6.865 and 9.180 (WTW).

2.2 Cyclic voltammetry (CV) and rotating disk electrode (RDE)

The CV and RDE experiments were performed in an 884 Professional VA instrument from Metrohm using a three-electrode set-up consisting in a glassy carbon electrode (diameter: 2 ± 0.1 mm) as working electrode (WE), platinum as counter electrode (CE) and an Ag/AgCl (3 M KCl) reference electrode (RE); all potentials where converted to reversible hydrogen electrode (RHE). The electrochemical surface area of the working electrode was determined as 0.035 ± 0.001 cm^2 with a Randles-Sevcik analysis of 10 mM $K_3Fe(CN)_6$ in 1.0 M KNO_3 using the diffusion coefficients reported on reference [34]. The glassy carbon electrode was used in stationary mode for CV and in hydrodynamic mode for RDE. The experiments were performed under normal atmosphere at 25°C and all the solutions were purged with N_2 for 20 minutes before the measurement. The data obtained with the RDE were processed with the software AfterMath (version 1.5.9888, Pine Research) in order to obtain the limiting currents at the different angular velocities.

2.3 Spectro-electrochemical analysis

Figure S1 in the Supporting Information presents the in-house-built spectro-electrochemical cell. The cell was placed inside a glovebox (GS Glovebox-System GS050912; < 1 ppm O_2) represented by the orange-colored line in the Figure S1a. The cell holder was printed with a 3D printer (3DWOX 1, Sindoh). The quartz cell had the following outer dimensions: width 20 × depth 10 × height 30 mm and an optical path length of 5 mm. For the electrochemical reduction of Tc(VII) a three-electrode arrangement was used. The WE was a glassy carbon rod (ALS Japan), the CE was a Pt wire (ALS Japan) and the RE was Ag/AgCl (3 M KCl) (ALS Japan). The electrodes were connected to a potentiostat (PGSTAT 101, Metrohm) outside the glovebox. An UV-vis spectrometer (AvaSpec-ULS2048 StarLine, Avantes) was located outside the glovebox along with the lamp (AvaLight-DH-S-BAL, Avantes) and both of them were connected to the cell holder using optical fiber.

The spectro-electrochemical experiments were carried out at 21°C. As general procedure, the sample was placed inside the cell and it was stirred throughout the entire experiment with a 5 mm magnetic stirrer. A potential staircase was applied varying the potential 0.01 V every four minutes (for example: –0.480 V for four minutes, then –0.490 V again for four minutes and so forth until –1 V vs Ag/AgCl or –0.790 V vs RHE). The starting potential of the staircase was –0.490 V vs Ag/AgCl at pH 2.0 and –0.620 V vs Ag/AgCl at pH 10.0. In parallel to the potential staircase, UV-vis spectra were continuously recorded (one spectrum every 30 seconds, i.e. 8 spectra per potential value) in the range from 200 to 1100 nm. The integration time was 10 ms and a background subtraction was performed using blanks of 2 M $NaClO_4$ at pH 2.0 and 10.0 depending on the sample. The 8 spectra obtained for each potential step were averaged in order to reduce the noise.

2.4 Solid analysis

After the complete reduction of Tc(VII) in the spectro-electrochemical cell at pH 2.0, a black solid was accumulated on the working electrode. The electrode was taken outside the solution and, when it got dry, the solid detached itself immediately and was collected for further study. The reduction in the spectro-electrochemical cell was repeated at pH 10.0 obtaining again a solid accumulated on the electrode that was also harvested. Both solid samples were studied by Raman microscopy, with a second batch of the solid obtained at pH 2.0 also being analyzed using scanning electron microscopy with energy dispersive X-ray spectroscopy (SEM-EDX) and X-ray photoelectron spectroscopy (XPS). Experimental conditions for Raman measurements [35] and for SEM-EDX and XPS [15] are described elsewhere and detailed in the supporting information.

The supernatant was analyzed by liquid scintillation counting (1414 LSC Winspectral α/β Wallac, Perkin Elmer; detection limit: 25 cpm. Measuring time: 10 minutes) finding that only 80 Bq out of the initial 321000 Bq remained in the solution, meaning that all Tc(VII) was reduced to the black Tc solid.

3. RESULTS AND DISCUSSION

3.1 Electrochemical Characterization, Cyclic Voltammetry (CV) and Rotating Disk Electrode (RDE)

Figure 1 shows the cyclic voltammograms of $NaClO_4$ solutions in absence (Figure 1a) and presence of Tc (Figure 1b) in the pH range from 2.0 to 10.0.

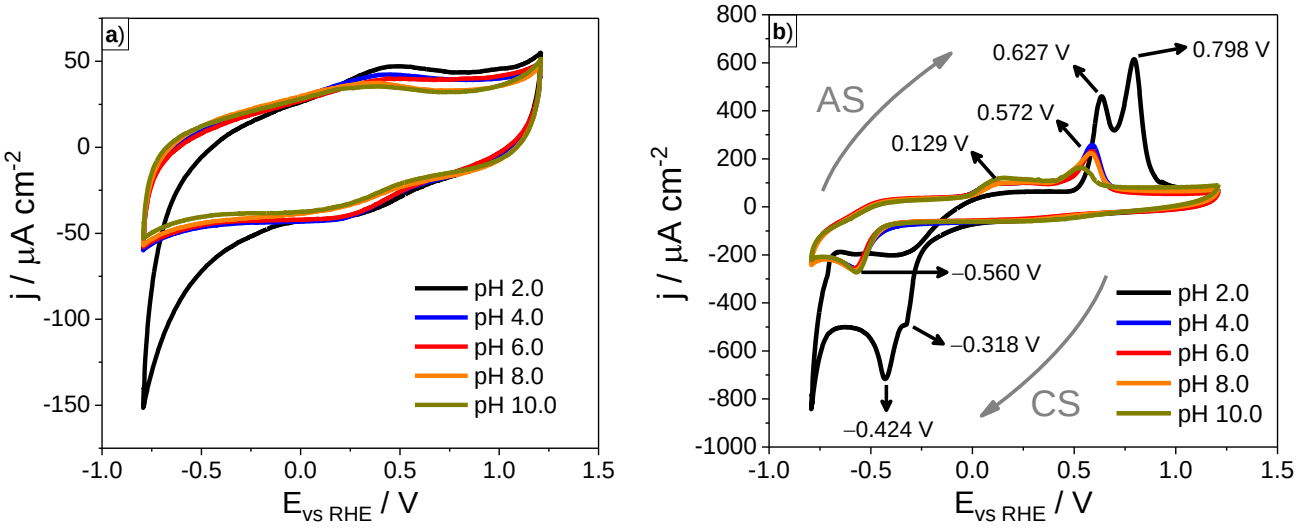

Figure 1. Cyclic voltammograms at 0.01 V s^{-1} scan rate in 2 M $NaClO_4$ under N_2 at different pH values a) in absence of Tc and b) in presence of 0.5 mM $KTcO_4$. Grey arrows represent the voltage scan direction of the cathodic scan (CS) and the anodic scan (AS).

As mentioned before, unlike chloride (Cl^-), perchlorate (ClO_4^-) does not form complexes with technetium [12]. In addition to that, the voltammogram of $NaClO_4$ (Figure 1a) shows only very small peaks close to 0.1 V vs. reversible hydrogen electrode (RHE) and some hydrogen evolution reaction potentials below –0.625 V at pH 2.0. In the presence of Tc, the voltammograms clearly change. Thus, the peaks in Figure 1b indicate the course of different oxidation states of technetium within the cycling voltammograms.

Two different Tc reduction behaviors can be spotted in the CVs depending on the pH in the cathodic scan. At pH 2.0 the system clearly shows two peaks during the reduction. A small peak at –0.318 V suggests the formation of an intermediary oxidation state, followed by a second reduction peak observed at –0.424 V. In contrast, at pH 4.0-10.0 one single cathodic peak at –0.560 V indicates a direct Tc(VII) reduction.

The voltammograms in Figure 1b show two anodic peaks despite the pH value, i.e. the formation of two Tc oxidation states. The potential of the reactions depends on the pH alike the reduction: while at pH 4.0 – 10.0 they behave in a similar way (anodic peaks at 0.129 V and 0.570 V), the peaks at pH 2.0 are shifted to more positive values (0.627 V and 0.789 V).

Although, the CVs provide already an idea on the mechanism of the Tc reduction and oxidation, they cannot be used for the determination of the exact amount of electrons transferred, due to the irreversibility of the process. For an improved understanding of the redox processes occurring, we combine cyclic voltammetry at different scan rates and the rotating disk electrode technique to apply the Randles-Sevcik and Levich equations for electrochemical data analysis. A full description of the equations and how to interpret them is defined as follows.

On one hand, by changing the scan rate of the CV, the peak currents can be analyzed with the Randles-Sevcik equation (Eq. [1]) [36,37]. It is assumed that all Tc remains dissolved and there is no precipitation or deposition on the electrode.

$$I_p = 2.69 \times 10^5 n^{3/2} A\, c\, D^{1/2} v^{1/2} \qquad [1]$$

where I_p is the peak current (A), n is the number of electrons transferred, A the area of the electrode (cm^2), c the analyte concentration (mol cm^{-3}), D the diffusion coefficient ($cm^2\ s^{-1}$), and u the CV scan rate ($V\ s^{-1}$). The terms n, A, c and D do not change here and can be grouped along with 2.69×10^5 in a new term Y. Therefore, Eq. [1] can be rewritten as Eq. [2].

When I_p is plotted *vs.* $u^{1/2}$ (Randles-Sevcik plot) a straight line with slope Y is obtained.

$$I_p = \mathrm{Y}\, v^{1/2} \qquad [2]$$

On the other hand, using a rotating disk electrode (RDE) the diffusion coefficients and the number of electrons can be determined. RDE is an experimental technique in which the working electrode rotates

on its own axis creating a laminar flow of the solution towards the electrode, improving the mass transport [38]. Such flow can be controlled by the angular velocity of the electrode and the behavior of the current is modelled using the Levich equation (Eq. [3]) [38].

$$I_L = (0.620)\, n\, F\, A\, \nu^{-1/6}\, D^{2/3}\, c\, \omega^{1/2} \qquad [3]$$

where I_L is the limiting current (A), which is the mass transport limited current obtained at the different rotation speed, n is the number of electrons transferred, F the Faraday constant (96 485.3329 C mol^{-1}), A the area of the electrode (cm^2), ν the kinematic viscosity of the electrolyte (cm^2 s^{-1}), D the diffusion coefficient of the species under study, i.e. the electroactive species (cm^2 s^{-1}), c the analyte concentration (mol cm^{-3}) and ω the angular velocity of the RDE (rads^{-1}). Alike Randles-Sevcik equation, n, A, ν, D and c can be grouped along with 0.620 F in B (Levich constant) and Eq. [3] can be summarized as Eq. [4].

$$I_L = B\, \omega^{1/2} \qquad [4]$$

When plotting I_L vs. $\omega^{1/2}$ (Levich plot) B is obtained from the slope of a linear fit and is used to determine the number of electrons transferred n or the diffusion coefficient D. In our system, we have approximated ν by 8.90×10^{-3} cm^2 s^{-1} corresponding to the kinematic viscosity of 2 M $NaClO_4$ in water [39]. The Tc concentration (0.5 mM) was low enough to neglect its effect on the viscosity.

Combining the slopes of the regression lines from the Randles-Sevcik and the Levich equations, two equations (Eq. [5] and Eq. [6]) are obtained for two unknown variables (D – the diffusion coefficient of Tc in 2 M $NaClO_4$ and n):

$$Y = 2.69 \times 10^5 A\, c\, D^{1/2}\, n^{3/2} \qquad [5]$$

$$B = 0.620\, F\, c\, A\, \nu^{-1/6}\, D^{2/3}\, n \qquad [6]$$

Solving this equation system, Eq. [7] and [8] were obtained, directly yielding D and n, respectively:

$$D = \left(\frac{\alpha E}{B}\right)^2 \qquad [7]$$

$$n = \frac{Y}{\alpha\, D^{3/2}} \qquad [8]$$

with $\alpha = 0.620\, F\, c\, A\, \upsilon^{-1/6}$, $E = (Y/\beta)^{3/2}$ and $\beta = 2.69 \times 10^5 A\, c$.

Since the reduction of Tc(VII) in $NaClO_4$ appears to follow the same mechanism throughout the pH range 4.0-10.0 according to Figure 1b, we selected pH 2.0 and pH 10.0 for the RDE experiments to encompass the working pH range by measuring the two extremes. The reduction curves of the systems at different angular velocities as well as the cyclic voltammograms at different scan rates are presented in Figures S2 and S3 in the supporting information. Figure 2 shows the Randles-Sevcik and Levich plots of Tc at pH 2.0 and 10.0. There is a clear linear correlation between I_L and $\omega^{1/2}$ as well as for I_p and $u^{1/2}$, and, therefore, the values for the slopes B and Y were replaced in Eq. [5] and [6] to obtain D and n at both pH values.

Table 1 summarizes the results of the electrochemical analysis.

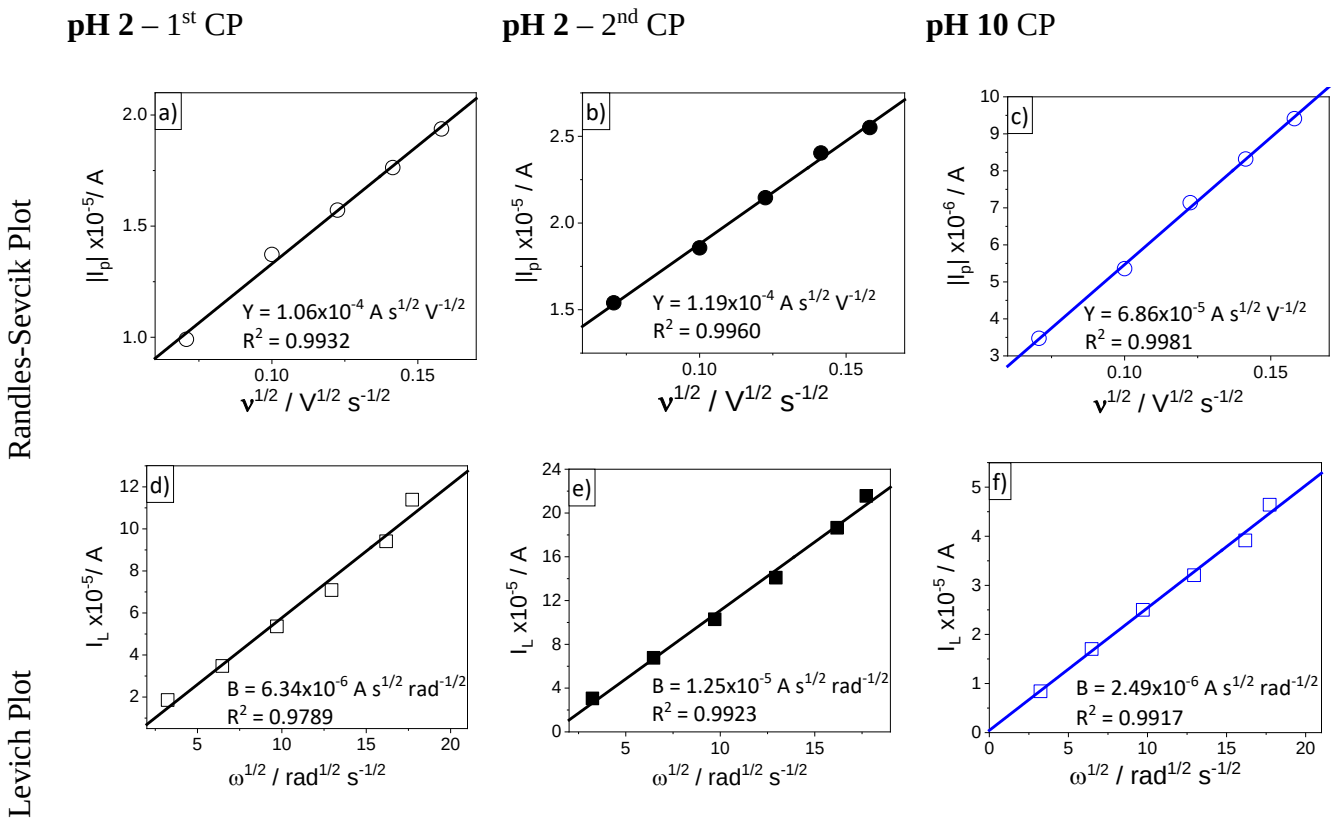

Figure 2. (circles) Randles-Sevcik and (squares) Levich plots of 0.5 mM $KTcO_4$ in 2 M $NaClO_4$ at different pH values. a), d) First cathodic peak (CP) at pH 2.0 (–0.318 V). b), e) Second cathodic peak (CP) at pH 2.0 (–0.424 V) c), f) Cathodic peak at pH 10.0 (–0.560 V). Y and B are the Randles-Sevcik and Levich slopes (Eq. [5] and [6] respectively).

Table 1. Reduction mechanism of Tc(VII) in $NaClO_4$ at pH 2.0 and pH 4.0-10.0 in their respective cathodic peaks (CP) and the associated reduction potential vs reversible hydrogen electrode ($E_{vs\ RHE}$).

CP \ pH	**2.0**	**4.0-10.0**
	Tc(VII) + 2.3 ± 0.3 e^- → Tc(V)	Tc(VII) + 3.2 ± 0.3 e^- → Tc(IV)
1	$D = 3.92\times10^{-5}\ cm^2\ s^{-1}$	$D = 5.75\times10^{-6}\ cm^2\ s^{-1}$
	$E_{vs\ RHE} = -0.318$ V	$E_{vs\ RHE} = -0.560$ V
	Tc(V) + 1.3 ± 0.3 e^- → Tc(IV)	
2	$D = 2.41\times10^{-4}\ cm^2\ s^{1}$	----
	$E_{vs\ RHE} = -0.424$ V	

n and *D* were calculated with Equations [7] and [8].

We have found that at pH 2.0 the reduction of Tc(VII) begins with the transfer of 2.3 ± 0.3 electrons yielding Tc(V) as an intermediary oxidation state that subsequently gains further 1.3 ± 0.3 electrons to become Tc(IV). At pH 10.0, the reduction of Tc(VII) is direct with the transfer of 3.2 ± 0.3 electrons to produce Tc(IV). The uncertainties in the number of errors were calculated using the error propagation method described elsewhere [40].

The electrochemical behavior displayed at pH 2.0 is in good agreement with the Latimer diagram of Tc under acidic conditions [41] where Tc(VI) is postulated as an intermediary oxidation state during the reduction from Tc(VII) to Tc(IV). However, as Tc(VI) is unstable in water, a rapid disproportionation to Tc(VII) and Tc(V) takes place [25,27,29]. This supports the electrochemical analysis (Table 1), suggesting that the small peak at -0.318 V at pH 2.0 is Tc(V). The potential shift with pH related to Tc(IV) formation (–0.424 V for pH 2 and –0.560 V for pH values 4.0, 6.0, 8.0 and 10.0) can be related to the difference in the pH, as it occurs, for example, with manganese where the reduction from $Mn(VII)O_4^-$ to $Mn(IV)O_2$ has a standard potential of 1.7 V at acidic pH and 0.60 V at alkaline pH, according to Mn Latimer diagrams [25].

The diffusion coefficients of the electroactive Tc species in $NaClO_4$ at pH 2.0 were determined as $3.92\times10^{-5}\ cm^2\ s^{-1}$ for Tc(VII) and $2.41\times10^{-4}\ cm^2\ s^{-1}$ for Tc(V). At pH 10.0, the diffusion coefficient of Tc(VII) is $5.75\times10^{-6}\ cm^2\ s^{-1}$. The starting Tc oxidation state at both pH 2.0 and pH 10.0 is Tc(VII), and, therefore, it is clear that pertechnetate is the electroactive species of the first cathodic peaks (CP) at both pH values. Previous studies on Tc diffusion coefficients in aqueous solution are extremely limited and no value could be found in the presence of a salt that remotely resembles $NaClO_4$ (like $KClO_4$ or

$NaBrO_4$). For the sake of comparison the values obtained in our work were contrasted against the diffusion coefficients of Tc in bentonite [42], where it was reported that the diffusion coefficient of pertechnetate decreases as pH increases, which is in well agreement with our findings with the RDE for the reduction mechanism of Tc(VII) (Table 1).

The oxidation mechanism could not be established because it was not possible to stabilize the reduced Tc aqueous species –theoretically Tc(IV)– at the begin of the experiment. As it will be shown in section *Solid Analysis*, the complete reduction of Tc(VII) led to the formation of a solid deposited on the working electrode (WE), making it impossible to apply the electrochemical analysis presented in this section as it is only feasible for species in solution. It is worth explaining that this issue did not affect the determination of the reduction mechanism because both the RDE and the CV experiments were fast enough to avoid the precipitation of the reduced Tc. However, the complete reduction of Tc(VII) necessary to start the RDE experiment for the oxidation takes several hours, giving enough time for the deposition of the reduced Tc solid. However, we can interpret that the second anodic peak (0.798 V at pH 2.0 and around 0.570 V at pH 4.0 – 10.0) in Figure 1b corresponds to the formation of Tc(VII), as this is the highest stable oxidation state in solution for technetium

3.2 In-situ spectro-electrochemical analysis of the Tc(VII) reduction

Spectro-electrochemical experiments were performed to follow the electrochemical reduction of $Tc(VII)O_4^-$ in $NaClO_4$ at both pH 2.0 and 10.0. The collected UV-vis spectra are shown in Figure 3. As expected, both spectral data sets display at the beginning of the experiments the characteristic signals of TcO_4^- at 247 and 289 nm [24]. With the application of the potential staircase, the intensity of these features gradually decreases until both bands finally disappear at the last potential steps, indicating full reduction of Tc(VII). The process was identical at both pH 2.0 and 10.0 (Figure 3 a and b).

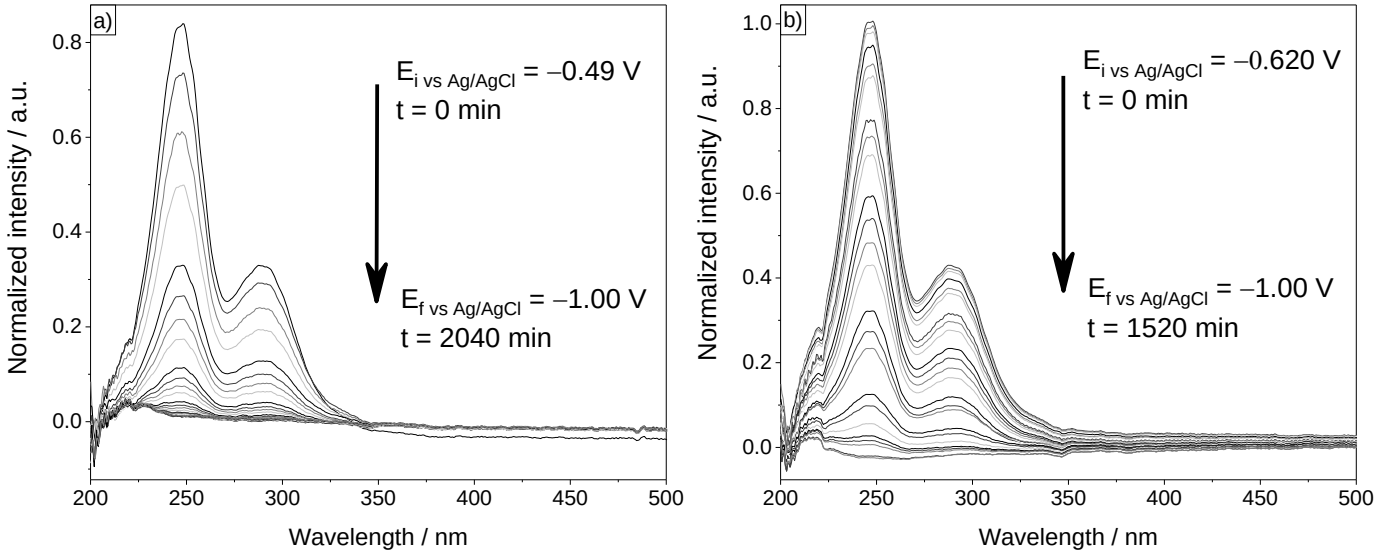

Figure 3. UV-vis spectra measured during the electrochemical reduction of 0.5 mM $Tc(VII)O_4^-$ in 2 M $NaClO_4$. a) pH 2.0. b) pH 10.0.

The complete reduction of Tc(VII) yielded a black solid deposited on the WE regardless of the sample pH. Taking into account, that UV-vis spectra confirm the lack of Tc(IV) chloride species with absorption at 234 nm and 338 nm [43], and that Tc(IV) is the final reduction product (Table 1), most likely the formed solid is a Tc(IV)-O species.

The spectroscopic behavior depicted in Figure 3b is in good agreement with the findings of the electrochemical analysis at pH 10.0 with no intermediary oxidation state between Tc(VII) and Tc(IV) during the reduction. Therefore, the occurrence of a Tc signal different from those of Tc(VII) was not expected. However, no spectroscopic evidence of the existence of the Tc(V) species suggested by the electrochemical analysis at pH 2.0 was found. This can be due to an extremely fast transition from Tc(V) to Tc(IV) or simply because the Tc(V) species is not active in the UV-vis range or its absorption coefficient is too low.

3.3 Solid analysis

In order to confirm the chemical identity of the solid obtained after the complete reduction of $Tc(VII)O_4^-$, Raman spectroscopy, XPS and SEM-EDX were performed. The Raman spectra of the solids at pH 2.0 and 10.0 are shown in Figure 4.

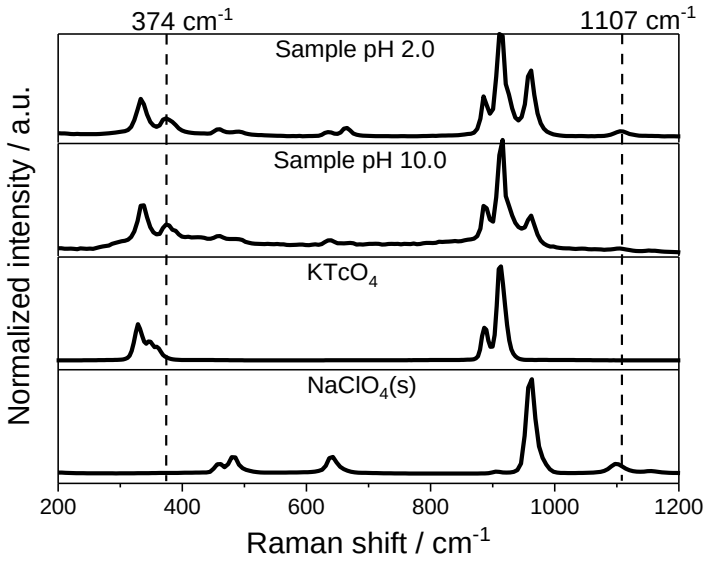

Figure 4. Raman spectra of the black solid obtained after the total reduction of 0.5 mM $KTcO_4$ in 2 M $NaClO_4$ at pH 2.0 and 10.0 in the spectro-electrochemical cell. The Raman spectra of $KTcO_4$ and $NaClO_4$ have been added for comparison.

It can be observed that the Raman spectra are identical for both samples, indicating that the chemical identity of the solids at both pH values is the same, supporting the results in Table 1. The spectra of the samples were compared with the spectra of $KTcO_4$ and $NaClO_4$. The bands at 458, 632, 666 and 960 cm^{-1} were attributed to sodium perchlorate [44] recrystallized on the working electrode along with the technetium solid.

The band at 330 cm^{-1} is assigned to Tc-O vibrations by comparison with the $KTcO_4$ spectra [45,46]. However, it is worth mentioning that according to the literature [43,47,48] the Tc-Cl bond presents two bands at 332 and 342 cm^{-1}. While no band around 340 cm^{-1} is present in the spectra of the samples, the bands appearing at 885 and 913 cm^{-1} are characteristic of the TcO_4^- structure corresponding to Tc-O vibrations [45,46]. Therefore, the band at 330 cm^{-1} is also assigned to the Tc-O vibration and no evidence of Tc-Cl bonding is present in the Raman spectra. This confirms that no interaction between Tc and chlorine species took place during the reduction.

Two bands at 374 and 1107 cm^{-1} remain unidentified after this assignment. Since the initial components of the samples were $KTcO_4$, $NaClO_4$ and water, these two remaining bands can be tentatively assigned to the reduced Tc solid that would be Tc(IV) according to the electroanalysis (Table 1). Previous works

[49,50] have reported a signal at 877 cm^{-1} for TcO_2 that does not appear in the Raman spectra of our samples. There is a possibility that this signal is overlapped by the band at 885 cm^{-1} but, as no reports for signals at 374 and 1107 cm^{-1} have been found for TcO_2, we refrain from characterizing the solid samples as technetium dioxide.

In order to confirm the oxidation state of technetium in the solid, XPS and SEM-EDX were applied. The XPS spectra of the solid evaluated in Tc *3d* and Cl *2p* is presented in Figure 5.

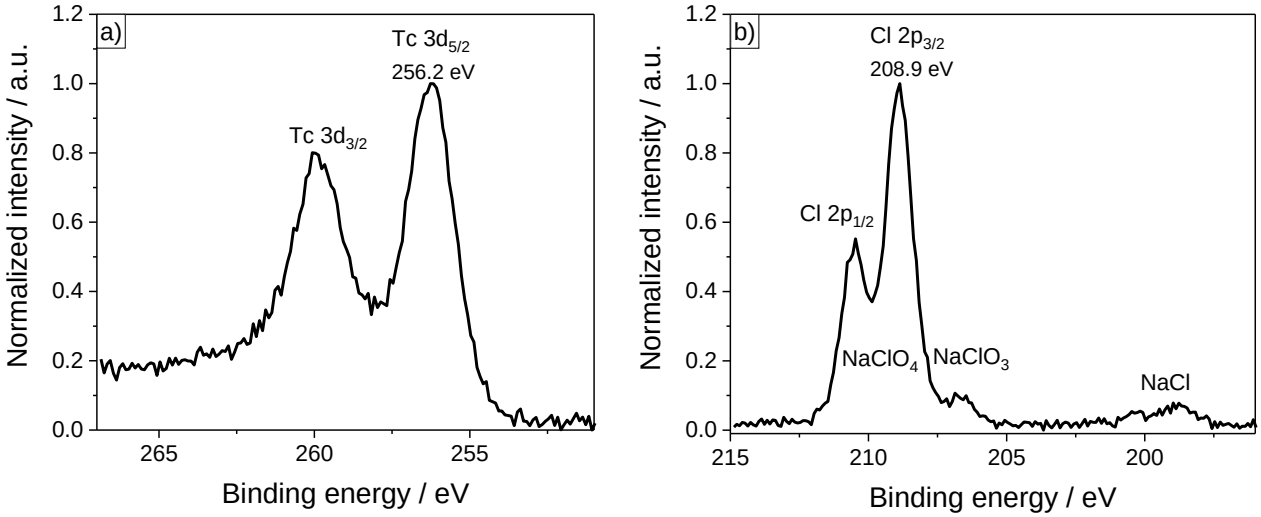

Figure 5. XPS spectra of the reduced Tc solid. s) Tc *3d*, b) Cl *2p*.

The Tc *3d* spectrum (Figure 5a) shows an intense Tc $3d_{5/2}$ peak at 256.2 eV assigned to Tc(IV) since it is close to the reference value for TcO_2 (256.8 eV [51]). $NaClO_4$ was present during the recording of the XPS spectra of the sample because no further separation or purification of the solid was performed after the reduction of Tc(VII) (see solid analysis in the experimental section). The Cl $2p_{3/2}$ elemental line of $NaClO_4$ is observed at 208.9 eV binding energy in accordance with its reference at 208.9 eV [52]. Since $NaClO_4$ degrades under X-ray irradiation and the charge of the sample surface caused by the XPS measurement will change slowly during degradation, charge referencing of elemental lines is not reliable if high degradation of $NaClO_4$ occurs. This was avoided by using monochromatic Al K_α X-rays, larger analysis area, and short acquisition time. Small portions of chlorite and chloride, i.e. the degradation products, are detected at the Cl *2p* spectrum (Figure 5b), making the results presented reliable despite the presence of $NaClO_4$.

Even though XPS cannot be used to establish the structure of the technetium compound, the oxidation state can be unequivocally assigned as Tc(IV). Therefore, the bands found at 374 and 1107 cm^{-1} in the

Raman spectra correspond to Tc(IV). To our knowledge, apart from the band at 877 cm^{-1} for TcO_2 [43], no other Raman signals for Tc(IV) have been reported before, making the results of this paper very relevant for the identification of Tc(IV) in other applications, e.g. Tc retention studies by minerals.

The SEM-EDX analysis is presented in Figure S4 in the supporting information. The morphology of the sample depicted in the micrographs shows three regions clearly separated: (1) mainly Na, Cl and O, (2) almost completely Tc and O and (3) indium from the foil on which the sample was prepared. This is consistent with the fact that ClO_4^- had no interaction with Tc and the solid obtained corresponds only to a reduced Tc species bonded to O.

4. CONCLUSIONS

The reduction of Tc(VII) in non-complexing media ($NaClO_4$) has been studied for the first time using spectro-electrochemical methods and electrochemical analysis, combined with other spectroscopic and microscopic techniques.

The electrochemical results show that the reaction mechanism depends on the pH. By applying Randles-Sevcik and Levich equations, the number of electrons during electrochemical analysis was determined. At pH 2.0, the reduction occurs in two steps with the initial gain of 2.3 ± 0.3 electrons by Tc(VII) to obtain Tc(V), which subsequently receives 1.3 ± 0.3 electrons to form Tc(IV). At pH 4.0-10.0 Tc(VII) is directly reduced to Tc(IV) with the transfer of 3.2 ± 0.3 electrons. The electrochemical reduction of Tc(VII) in $NaClO_4$ was followed in parallel with UV-vis absorption spectroscopy. Even though no spectroscopic evidence of intermediate Tc(V) could be obtained, UV-vis showed the absence of Tc(IV)-chloride species. After the total reduction of Tc(VII) at both pH 2.0 and 10.0, a black solid was formed. Raman spectroscopy confirmed that both solids had the same chemical identity despite the initial pH value, whereas SEM-EDX analysis proves that the solid only consists of Tc and O. XPS analysis identified the solids as Tc(IV) and agrees with the obtained CV results and the electrochemical analysis.

In addition to an accurate determination of the electrons transferred in the reduction process depending on the pH, this study has also yielded two Raman signals at 374 and 1107 cm^{-1} that correspond to the Tc(IV) species formed after the total reduction of Tc(VII). Such Raman features will be relevant to specific questions in environmental engineering for the identification of Tc(IV) compounds that are the products of the reductive immobilization of Tc(VII) by common minerals and could only be identified by the use of more expensive spectroscopies.

This work presents fundamental data to understand Tc redox chemistry and its dependence on pH under the simplest aqueous conditions, i.e. in a non-complexing media.

Both results and methodology applied in the electrochemical analysis will serve as valuable references for further studies to identify Tc redox chemistry in complex systems, e.g. in presence of inorganic and organic ligands. These fundamental studies are essential for a realistic and broad picture of the Tc chemical redox and complexation behavior. A basic Tc chemical understanding will also provide a direct impact on environment protection by enhancing Tc remediation strategies in contaminated areas as well as for the safety assessment of nuclear waste repositories.

Furthermore, this work is also the first step towards a future development of spectro-electrochemical techniques. We envision the development of spectro-electrochemistry couplings to characterize the structure of redox-active species at different oxidation states, which will be helpful not only for Tc but also for other redox-active elements whose chemical behavior is still to be fully defined.

Abbreviations

CE: counter electrode
CP: Cathodic peak
CV: Cyclic voltammetry
RDE: Rotating disk electrode
RE: reference electrode
RHE: Reversible hydrogen electrode
SEM-EDX: Scanning electron microscopy with energy dispersive X-ray spectroscopy
WE: working electrode
XPS: X-ray photoelectron spectroscopy

Supporting Information. In-house built spectro-electrochemical cell. Reduction curves. CVs at different scan rates. SEM-EDX. Experimental description of Tc solid analysis.

Acknowledgment

We are very grateful to Susana Jiménez and Stephan Weiß for their help in the lab. We acknowledge the German Federal Ministry for Economic Affairs and Climate Action (former German Federal Ministry of Economic Affairs and Energy) for the VESPA II joint project (02E11607B).

References

(1) Perrier, C.; Segrè, E. Radioactive Isotopes of Element 43. *Nature* **1937**, *140* (3535), 193–194. https://doi.org/10.1038/140193b0.

(2) Herbert, R.; Kulke, P. W.; Shepherd, R. T. H. The Use of Technetium 99m as a Clinical Tracer Element. *Postgrad. Med. J.* **1965**, *41* (481), 656–662. https://doi.org/10.1136/pgmj.41.481.656.

(3) Meena, A. H.; Arai, Y. Environmental Geochemistry of Technetium. *Environ. Chem. Lett.* **2017**, *15* (2), 241–263. https://doi.org/10.1007/s10311-017-0605-7.

(4) Momoshima, N.; Sayad, M.; Yamada, M.; Takamura, M.; Kawamura, H. Global Fallout Levels of ^{99}Tc and Activity Ratio of ^{99}Tc/^{137}Cs in the Pacific Ocean. *J. Radioanal. Nucl. Chem.* **2005**, *266* (3), 455–460. https://doi.org/10.1007/s10967-005-0931-2.

(5) Guérin, B.; Tremblay, S.; Rodrigue, S.; Rousseau, J. A.; Dumulon-Perreault, V.; Lecomte, R.; van Lier, J. E.; Zyuzin, A.; van Lier, E. J. Cyclotron Production of ^{99m}Tc: An Approach to the Medical Isotope Crisis. *J. Nucl. Med.* **2010**, *51* (4), 13N-16N.

(6) Jurisson, S.; Gawenis, J.; Landa, E. R. Sorption of ^{99m}Tc Radiopharmaceutical Compounds by Soils. *Health Phys.* **2004**, *87* (4).

(7) Icenhower, J. P.; Qafoku, N. P.; Zachara, J. M.; Martin, W. J. The Biogeochemistry of Technetium: A Review of the Behavior of an Artificial Element in the Natural Environment. *Am. J. Sci.* **2010**, *310* (8), 721–752. https://doi.org/10.2475/08.2010.02.

(8) Lear, G.; McBeth, J. M.; Boothman, C.; Gunning, D. J.; Ellis, B. L.; Lawson, R. S.; Morris, K.; Burke, I. T.; Bryan, N. D.; Brown, A. P.; Livens, F. R.; Lloyd, J. R. Probing the Biogeochemical Behavior of Technetium Using a Novel Nuclear Imaging Approach. *Environ. Sci. Technol.* **2010**, *44* (1), 156–162. https://doi.org/10.1021/es802885r.

(9) Lieser, K. H.; Bauscher, C. Technetium in the Hydrosphere and in the Geosphere. I Chemistry of Technetium and Iron in Natural Waters and Influence of the Redox Potential on the Sorption of Technetium. *Radiochim. Acta* **1987**, *42*, 205–213.

(10) Masters-Waage, N. K.; Morris, K.; Lloyd, J. R.; Shaw, S.; Mosselmans, J. F. W.; Boothman, C.; Bots, P.; Rizoulis, A.; Livens, F. R.; Law, G. T. W. Impacts of Repeated Redox Cycling on Technetium Mobility in the Environment. *Environ. Sci. Technol.* **2017**, *51* (24), 14301–14310. https://doi.org/10.1021/acs.est.7b02426.

(11) Corkhill, C. L.; Bridge, J. W.; Chen, X. C.; Hillel, P.; Thornton, S. F.; Romero-Gonzalez, M. E.; Banwart, S. A.; Hyatt, N. C. Real-Time Gamma Imaging of Technetium Transport through Natural and Engineered Porous Materials for Radioactive Waste Disposal. *Environ. Sci. Technol.* **2013**,

47 (23), 13857–13864. https://doi.org/10.1021/es402718j.

(12) Grenthe, I.; Gaona, X.; Plyasunov, A. V.; Rao, L.; Runde, W. H.; Grambow, B.; Konings, R. J. M.; Smith, A. L.; Moore, E. E. *Second Update on the Chemical Thermodynamics of Uranium, Neptunium, Plutonium, Americium and Technetium*; OECD Nuclear Energy Agency Data Bank: Boulogne-Billancourt, France, 2020.

(13) Rodríguez, D. M.; Mayordomo, N.; Scheinost, A. C.; Schild, D.; Brendler, V.; Müller, K.; Stumpf, T. New Insights on the ^{99}Tc(VII) Removal by Pyrite: A Spectroscopic Approach. *Environ. Sci. Technol.* **2020**, *54*, 2678–2687.

(14) Huo, L.; Xie, W.; Qian, T.; Guan, X.; Zhao, D. Reductive Immobilization of Pertechnetate in Soil and Groundwater Using Synthetic Pyrite Nanoparticles. *Chemosphere* **2017**, *174*, 456–465. https://doi.org/10.1016/j.chemosphere.2017.02.018.

(15) Rodríguez, D. M.; Mayordomo, N.; Schild, D.; Shams Aldin Azzam, S.; Brendler, V.; Müller, K.; Stumpf, T. Reductive Immobilization of ^{99}Tc(VII) by FeS2: The Effect of Marcasite. *Chemosphere* **2021**, *281*, 130904. https://doi.org/https://doi.org/10.1016/j.chemosphere.2021.130904.

(16) Schmeide, K.; Rossberg, A.; Bok, F.; Shams Aldin Azzam, S.; Weiss, S.; Scheinost, A. C. Technetium Immobilization by Chukanovite and Its Oxidative Transformation Products : Neural Network Analysis of EXAFS Spectra. *Sci. Total Environ.* **2021**, *770*, 145334. https://doi.org/10.1016/j.scitotenv.2021.145334.

(17) Yalçıntaş, E.; Scheinost, A. C.; Gaona, X.; Altmaier, M. Systematic XAS Study on the Reduction and Uptake of Tc by Magnetite and Mackinawite. *Dalt. Trans.* **2016**, *45* (44), 17874–17885. https://doi.org/10.1039/C6DT02872A.

(18) Marshall, T. A.; Morris, K.; Law, G. T. W.; Mosselmans, J. F. W.; Bots, P.; Parry, S. A.; Shaw, S. Incorporation and Retention of ^{99}Tc(IV) in Magnetite under High pH Conditions. *Environ. Sci. Technol.* **2014**, *48* (20), 11853–11862. https://doi.org/10.1021/es503438e.

(19) Mayordomo, N.; Rodríguez, D. M.; Rossberg, A.; Foerstendorf, H.; Heim, K.; Brendler, V.; Müller, K. Analysis of Technetium Immobilization and Its Molecular Retention Mechanisms by Fe(II)-Al(III)-Cl Layered Double Hydroxide. *Chem. Eng. J.* **2021**, *408*, 127265. https://doi.org/10.1016/j.cej.2020.127265.

(20) Chotkowski, M.; Czerwiński, A. *Electrochemistry of Technetium*; Monographs in Electrochemistry; Springer International Publishing: Cham, 2021. https://doi.org/10.1007/978-3-030-62863-5.

(21) Chotkowski, M.; Czerwiński, A. Electrochemical and Spectroelectrochemical Studies of

Pertechnetate Electroreduction in Acidic Media. *Electrochim. Acta* **2012**, *76*, 165–173. https://doi.org/10.1016/j.electacta.2012.04.123.

(22) Chotkowski, M.; Czerwiński, A. Thin Layer Spectroelectrochemical Studies of Pertechnetate Reduction on the Gold Electrodes in Acidic Media. *Electrochim. Acta* **2014**, *121*, 44–48. https://doi.org/https://doi.org/10.1016/j.electacta.2013.12.142.

(23) Chotkowski, M.; Wrzosek, B.; Grdeń, M. Intermediate Oxidation States of Technetium in Concentrated Sulfuric Acid Solutions. *J. Electroanal. Chem.* **2018**, *814*, 83–90. https://doi.org/10.1016/j.jelechem.2018.02.042.

(24) Paquette, J.; Lawrence, W. E. A Spectroelectrochemical Study of the Technetium(IV)/Technetium(III) Couple in Bicarbonate Solutions. *Can. J. Chem* **1985**, *63* (Iv), 2369–2373.

(25) Chatterjee, S.; Hall, G. B.; Johnson, I. E.; Du, Y.; Walter, E. D.; Washton, N. M.; Levitskaia, T. G. Surprising Formation of Quasi-Stable Tc(VI) in High Ionic Strength Alkaline Media. *Inorg. Chem. Front.* **2018**, *5* (9), 2081–2091. https://doi.org/10.1039/c8qi00219c.

(26) Kuznetsov, V. V; Chotkowski, M.; Poineau, F.; Volkov, M. A.; German, K.; Filatova, E. A. Technetium Electrochemistry at the Turn of the Century. *J. Electroanal. Chem.* **2021**, *893* (April), 115284. https://doi.org/10.1016/j.jelechem.2021.115284.

(27) Salaria, G. B. S.; Rulfs, C. L.; Elving, P. J. 456. Polarographic Behaviour of Technetium. *J. Chem. Soc.* **1963**, No. 0, 2479–2484. https://doi.org/10.1039/JR9630002479.

(28) Salaria, G. B. S.; Rulfs, C. L.; Elving, P. J. Polarographic and Coulometric Determination of Technetium. *Anal. Chem.* **1963**, *35* (8), 979–982. https://doi.org/10.1021/ac60201a018.

(29) Grassi, J.; Devynck, J.; Trémillon, B. Electrochemical Studies of Technetium at a Mercury Electrode. *Anal. Chim. Acta* **1979**, *107* (C), 47–58. https://doi.org/10.1016/S0003-2670(01)93194-0.

(30) Colton, R.; Dalziel, J.; Griffith, W. P.; Wilkinson, G. 15. Polarographic Study of Manganese, Technetium, and Rhenium. *J. Chem. Soc.* **1960**, No. 0, 71–78. https://doi.org/10.1039/JR9600000071.

(31) Colton, R.; Peacock, R. D. An Outline of Technetium Chemistry. *Q. Rev. Chem. Soc.* **1962**, *16* (4), 299–315. https://doi.org/10.1039/QR9621600299.

(32) Astheimer, L.; Schwochau, K. Zur Polarographie Des Technetiums: I. Gleichstrom- Und Wechselstrompolarographische Untersuchungen an Pertechnetat-Lösungen. *J. Electroanal. Chem.* **1964**, *8* (5), 382–389. https://doi.org/https://doi.org/10.1016/0022-0728(64)80072-3.

(33) Poineau, F.; Fattahi, M.; Den Auwer, C.; Hennig, C.; Grambow, B. Speciation of Technetium and

Rhenium Complexes by in Situ XAS-Electrochemistry. *Radiochim. Acta* **2006**, *94* (5), 283–289. https://doi.org/10.1524/ract.2006.94.5.283.

(34) Ameur, Z. O.; Husein, M. M. Electrochemical Behavior of Potassium Ferricyanide in Aqueous and (w/o) Microemulsion Systems in the Presence of Dispersed Nickel Nanoparticles. *Sep. Sci. Technol.* **2013**, *48* (5), 681–689. https://doi.org/10.1080/01496395.2012.712594.

(35) Mayordomo, N.; Rodríguez, D. M.; Schild, D.; Molodtsov, K.; Johnstone, E. V.; Hübner, R.; Shams Aldin Azzam, S.; Brendler, V.; Müller, K. Technetium Retention by Gamma Alumina Nanoparticles and the Effect of Sorbed Fe^{2+}. *J. Hazard. Mater.* **2020**, *388*, 122066. https://doi.org/10.1016/j.jhazmat.2020.122066.

(36) Brett, C. M. A.; Brett, A. M. O. *Electrochemistry : Principles, Methods, and Applications*; Oxford University Press, 1993.

(37) Brett, C. M. A.; Brett, A. M. O. *Electroanalysis*; Oxford University Press, 1998.

(38) Du, C.; Tan, Q.; Yin, G.; Zhang, J. 5 - Rotating Disk Electrode Method. In *Rotating Electrode Methods and Oxygen Reduction Electrocatalysts*; Xing, W., Yin, G., Zhang, J. B. Eds.; Elsevier: Amsterdam, 2014; pp 171–198. https://doi.org/https://doi.org/10.1016/B978-0-444-63278-4.00005-7.

(39) Nightingale, E. R. Viscosity of Aqueous Sodium Perchlorate Solutions. *J. Phys. Chem.* **1959**, *63* (5), 742–743. https://doi.org/10.1021/j150575a025.

(40) Andraos, J. On the Propagation of Statistical Errors for a Function of Several Variables. *J. Chem. Educ.* **1996**, *73*, 150–154.

(41) Bard, A. J.; Parsons, R.; Jordan, J. *Standard Potentials in Aqueous Solution*; Marcel Dekker, Inc.: New York, 1985.

(42) Wang, X.; Tao, Z. Diffusion of $^{99}TcO_4^-$ in Compacted Bentonite: Effect of PH, Concentration, Density and Contact Time. *J. Radioanal. Nucl. Chem.* **2004**, *260* (2), 305–309. https://doi.org/10.1023/b:jrnc.0000027101.01834.1b.

(43) Ben Said, K.; Fattahi, M.; Musikas, C.; Revel, R.; Abbé, J. C. The Speciation of Tc(IV) in Chloride Solutions. *Radiochim. Acta* **2000**, *88* (9–11), 567–571. https://doi.org/10.1524/ract.2000.88.9-11.567.

(44) Lafuente, B.; Downs, R. T.; Yan, H.; Stone, N. The Power of Databases: The RRUFF Project. In *Highlights in Mineralogical Crystallography*; De Gruyter: Berlin, 2015; pp 1–30.

(45) Nakamoto, K. *Infrared and Raman Spectra of Inorganic and Coordination Compounds*; John Wiley & Sons, Inc.: Hoboken, NJ, USA, 2008. https://doi.org/10.1002/9780470405840.

(46) Weaver, J.; Soderquist, C. Z.; Washton, N. M.; Lipton, A. S.; Gassman, P. L.; Lukens, W. W.;

Kruger, A. A.; Wall, N. A.; Mccloy, J. S. Chemical Trends in Solid Alkali Pertechnetates. *Inorg. Chem.* **2017**, *56*, 2533–2544. https://doi.org/10.1021/acs.inorgchem.6b02694.

(47) Thomas, R. W.; Heeg, M. J.; Elder, R. C.; Deutsch, E. Structural (EXAFS) and Solution Equilibrium Studies on the Oxotechnetium(V) Complexes TcO_{X4}^- and $TcOX_5^{2-}$ (X = Cl, Br). *Inorg. Chem.* **1985**, *24* (10), 1472–1477. https://doi.org/10.1021/ic00204a014.

(48) Schwochau, K.; Krasser, W. Schwingungsspektren und Kraftkonstanten der Hexahalogeno-Komplexe des Technetium(IV) und Rhenium(IV). *Zeitschrift für Naturforsch. A* **1969**, *24* (3), 403–407. https://doi.org/doi:10.1515/zna-1969-0316.

(49) Gu, B.; Ruan, C. Determination of Technetium and Its Speciation by Surface-Enhanced Raman Spectroscopy. *Anal. Chem.* **2007**, *79* (6), 2341–2345. https://doi.org/10.1021/ac062052y.

(50) Mikelsons, M. V.; Pinkerton, T. C. Raman Spectroscopic Evidence for Tc-Oxo Cores in Tc-HEDP Complexes. *Int. J. Radiat. Appl. Instrumentation. Part* **1987**, *38* (7), 569–570. https://doi.org/10.1016/0883-2889(87)90206-1.

(51) *NIST X-Ray Photoelectron Spectroscopy Database, Version 4.1*; National Institute of Standards and Technology (NIST): Gaithersburg, USA, 2012.

(52) Beard, B. C. Sodium Salts of Chlorine Oxyacid Anions, Cl(+7), Perchlorate, XPS Comparison Spectra. *Surface science spectra.* **1993**, (2)2, 97–103. https://doi.org/10.1116/1.1247738.